Polymer 49 (2008) 2578–2586

Contents lists available at ScienceDirect

Polymer

journal homepage: www.elsevier.com/locate/polymer

Relationship between biaxial orientation and oxygen permeability of polypropylene film

Y.J. Lin [a], P. Dias [a], H.Y. Chen [b], A. Hiltner [a,*], E. Baer [a]

[a] Department of Macromolecular Science and Engineering and Center for Applied Polymer Research, Case Western Reserve University, Cleveland, OH 44106-7202, United States
[b] New Products – Materials Science, Core R&D, The Dow Chemical Company, Freeport, TX 77541, United States

ARTICLE INFO

Article history:
Received 5 February 2008
Received in revised form 17 March 2008
Accepted 19 March 2008
Available online 27 March 2008

Keywords:
Polypropylene
Biaxial orientation
Oxygen permeability

ABSTRACT

Biaxially oriented polypropylene (BOPP) films were produced by simultaneous and sequential biaxial stretching to various balanced and unbalanced draw ratios. The BOPP films were characterized in terms of density, crystallinity, refractive index, oxygen permeability and dynamic mechanical relaxation behavior. It was found that the density and crystallinity of BOPP films decreased as the area draw ratio increased. Sequential stretching led to a slightly lower density than simultaneous stretching to the same draw ratio. Moreover, sequential stretching produced lower orientation in the first stretch direction and higher orientation in the second stretch direction compared to simultaneous stretching. The study confirmed the generality of a one-to-one correlation between the oxygen permeability of BOPP films and the mobility of amorphous tie chains as measured by the intensity of the dynamic mechanical β-relaxation. Moreover, the study established the correlation for commercially important sequentially drawn BOPP films with an unbalanced draw ratio. Finally, the chain mobility in the stretch direction was found to depend on the final stress during stretching.

1. Introduction

Two of the key requirements for packaging films in beverage and food applications are atmosphere control and mechanical robustness. For polypropylene, adequate properties are achieved commercially through tentering processes that enhance toughness and gas barrier [1,2]. Commercial biaxially oriented polypropylene (BOPP) films are usually produced through a sequential process with unbalanced draw ratios. In this situation, an unoriented starting sheet is first stretched uniaxially at the softening temperature and then stretched in the perpendicular direction at elevated temperature. However, recent technological advances have allowed for simultaneous biaxial drawing on a commercial scale where unoriented extrudate can be stretched in two perpendicular directions in one step, resulting in a more energy and time-efficient process [3]. As a consequence, it is of immediate interest to compare and contrast the solid state structure and properties achieved with the two methods for fabricating BOPP film.

The first step in the sequential process is uniaxial stretching in the machine direction under constrained conditions. As described by Lüpke et al. [4], the initially unoriented film is transformed into a highly oriented, fibrous structure of the shish–kabob type. The crystal orientation is dominated by uniaxial *c*-axis orientation in the stretch direction. In the second step, the initial morphological response to the transverse stretch is separation and splaying of the close-packed shish–kabob fibers, and formation of a population of thin fibrils highly oriented in the transverse direction. As the transverse stretch increases, the shish–kabob fibers are completely transformed into a purely fibrous network with *c*-axes preferentially oriented in the two orthogonal stretch directions [4–6]. One study that also considered the amorphous phase found that the amorphous chains are oriented almost entirely in second stretch direction [7].

Because sequential stretching produces different fibrous structures in the first and second stretch directions, a balanced biaxial draw ratio results in significantly higher orientation in the second stretch direction [4]. It is not surprising that the stress–strain behavior is anisotropic as well. In order to obtain a good balance in properties, tentered BOPP is typically fabricated with different draw ratios, and with different stretch temperatures, in the machine and transverse directions.

In contrast, simultaneous biaxial stretching produces a fibrillar network texture in a single step [8]. Isotropic orientation of the

* Corresponding author. Department of Macromolecular Science and Engineering and Center for Applied Polymer Research, Case Western Reserve University, Kent Hale Smith Building, Room 423, 10900 Euclid Avenue, Cleveland, OH 44106-7202, United States.
E-mail address: ahiltner@case.edu (A. Hiltner).

0032-3861/$ – see front matter © 2008 Elsevier Ltd. All rights reserved.
doi:10.1016/j.polymer.2008.03.033

c-axes [9,10], differentiates the single step BOPP film from the sequentially stretched film with bimodal *c*-axis orientation. As a consequence, a simultaneously stretched film with a balanced draw ratio possesses isotropic properties, which further distinguishes it from the sequentially stretched counterpart.

It is not known whether the morphological differences between sequentially and simultaneously drawn films also impact the gas permeability. Few studies have addressed the fundamental relationships between the solid state structure of BOPP films and the gas permeability. Gas transport is seen as occurring only through the amorphous regions. Consequently, gas permeability does not exhibit a simple relationship with optical birefringence, which is dominated by orientation of the crystalline phase [11]. However, one report, with very limited data, showed a correlation between oxygen permeability and Herman's amorphous phase orientation function in the transport direction [12].

The orientation process for forming BOPP film stretches and tightens the amorphous tie molecules that connect the crystals and transfer the stress. This suggests that the morphological rearrangements during stretching lead to restricted motion of the amorphous chains. Recent studies of simultaneously drawn BOPP films with a balanced draw ratio found a single one-to-one correlation between the oxygen permeability and the intensity of the dynamic mechanical β-relaxation, which arises from main chain motions in the amorphous phase. The correlation encompassed BOPP films obtained from different isotactic propylene homopolymers and copolymers [13], and BOPP films obtained by stretching PP sheets with different thermal histories [14].

It needs to be determined if the correlation extends to the commercially important sequentially drawn BOPP film with an unbalanced draw ratio. In the present study, PP sheet is drawn sequentially and simultaneously with balanced and unbalanced draw ratios. Correlations are sought between the oxygen permeability of the BOPP films and the amorphous chain mobility.

2. Materials and methods

The polymer used in this study was a developmental polypropylene that was prepared with a post-metallocene catalyst by The Dow Chemical Company. It had weight average molecular weight M_w of 3.42×10^5 g mol^{-1} and M_w/M_n of 2.9. Unoriented sheets with a thickness of approximately 0.6 mm were prepared by compression molding. Polypropylene pellets were molded at 190 °C using a laboratory hot press and quenched as described previously [14].

Square specimens 85 mm × 85 mm were cut from the compression molded sheets, marked with a grid pattern, and biaxially stretched in a Brückner Karo IV biaxial stretcher at 140 °C at an engineering strain rate of 400% s^{-1} based on the original specimen dimensions. The preheat time before stretching was fixed to be 1 min. Stretching was performed either simultaneously in the two directions or sequentially. In simultaneous stretching to different draw ratios, the sheet was stretched in both directions to the lower draw ratio. Then, while the film was constrained at the lower draw ratio, it was stretched further to the higher draw ratio. In sequential stretching, the specimen was constrained in one direction and stretched in the other direction; after that, it was constrained in the first stretch direction and stretched in the second direction. Load and displacement were recorded and the stress–strain curves were calculated from these data. The uniformity of the drawn specimens was determined from the even deformation of the grid pattern.

Specimens weighing 5–10 mg were cut from the molded sheet or the biaxially stretched film. The first heating thermograms were recorded at a heating rate of 10 °C min^{-1} from −60 to 190 °C.

The density was measured at 23 °C according to ASTM D1505-85. A 2-propanol/water gradient column with a range of 0.85–0.95 g cm^{-3} was calibrated with glass floats with known density. Small pieces of film (~2 mm × 2 mm) were placed in the column and measurements were taken after 10 h equilibration. At least 3 pieces from each film were tested. The error in the density measurements was ±0.0005.

A Metricon Model 2010 Prism-Coupler was used to measure the refractive index of the oriented films at a wavelength of 1544 nm. The measurements were performed at 23 °C.

Oxygen flux $J(t)$ at 0% relative humidity, 1 atm and 23 °C was measured with a MOCON OX-TRAN 2/20. The permeant gas stream was diluted with nitrogen to achieve a 2% oxygen concentration in order to avoid exceeding the detector capability of the instrument. Permeability was obtained from the steady flux J_o according to

$$P = J_o l/p \quad (1)$$

where p is the oxygen pressure and l is the film thickness. Two films prepared under the same conditions were tested to obtain the average permeability. The error in the permeability measurement was about 5%.

A dynamic mechanical thermal analyzer (DMTA) Mk II unit from Polymer Laboratories was used to obtain tan δ. Specimens cut parallel to the two stretching directions were tested in the tensile mode with a frequency of 1 Hz and a strain of 0.085% over the temperature range from −60 to 120 °C with a heating rate of 3 °C min^{-1}.

3. Results and discussion

3.1. Biaxial stress–strain behavior

A thermogram of the compression molded PP sheet showed the gradual onset of melting at about 120 °C and the peak melting temperature at 146 °C. At 140 °C, the temperature used to perform the stretching, the sheet was partially melted. Stretching at lower temperatures required larger forces and often resulted in void formation. With increasing temperature, the stress response decreased as the crystals melted. However, as more crystals melted, the tie chains became less effective and the amount of orientation was reduced. An optimum balance in stress response and orientation was achieved for this resin at 140 °C [14]. The sheet was preheated at 140 °C for 60 s and stretched at a strain rate of 400% s^{-1}.

Typical stress–strain curves for simultaneous biaxial stretching are shown in Fig. 1. In these examples, the target draw ratio in the *x*-direction λ_x was constant and equal to 5, whereas the draw ratio in the *y*-direction λ_y was varied from 3 to 7. In simultaneous stretching, the sheet was stretched in both directions to the lower draw ratio. The stress–strain curves, which of course were essentially the same in the two directions, showed yielding at a draw ratio of about 1.1 followed by strain hardening. Then, while the film was constrained at the lower draw ratio in the *x*-direction, it was stretched further to the higher draw ratio in the *y*-direction. During this stretching, the film strain-hardened further in the stretched direction, whereas in the constrained direction, the stress relaxed slightly before some further strain-hardening occurred due to the constraint.

In sequential stretching, Fig. 2, the film was stretched in the *x*-direction to a target draw ratio of 5 while being constrained in the *y*-direction. After a pause of 0.4 s that was imposed by the instrument, the film was stretched in the *y*-direction to the target draw ratio while being constrained in the *x*-direction. During the first stretch, yielding occurred in the *x*-direction, and in the *y*-direction as well due to the stress imposed by the constraint. The stress relaxed somewhat during the 0.4 s pause, and then increased during the second stretching in both the stretched and constrained directions due to strain hardening. In all cases, the final stress in the

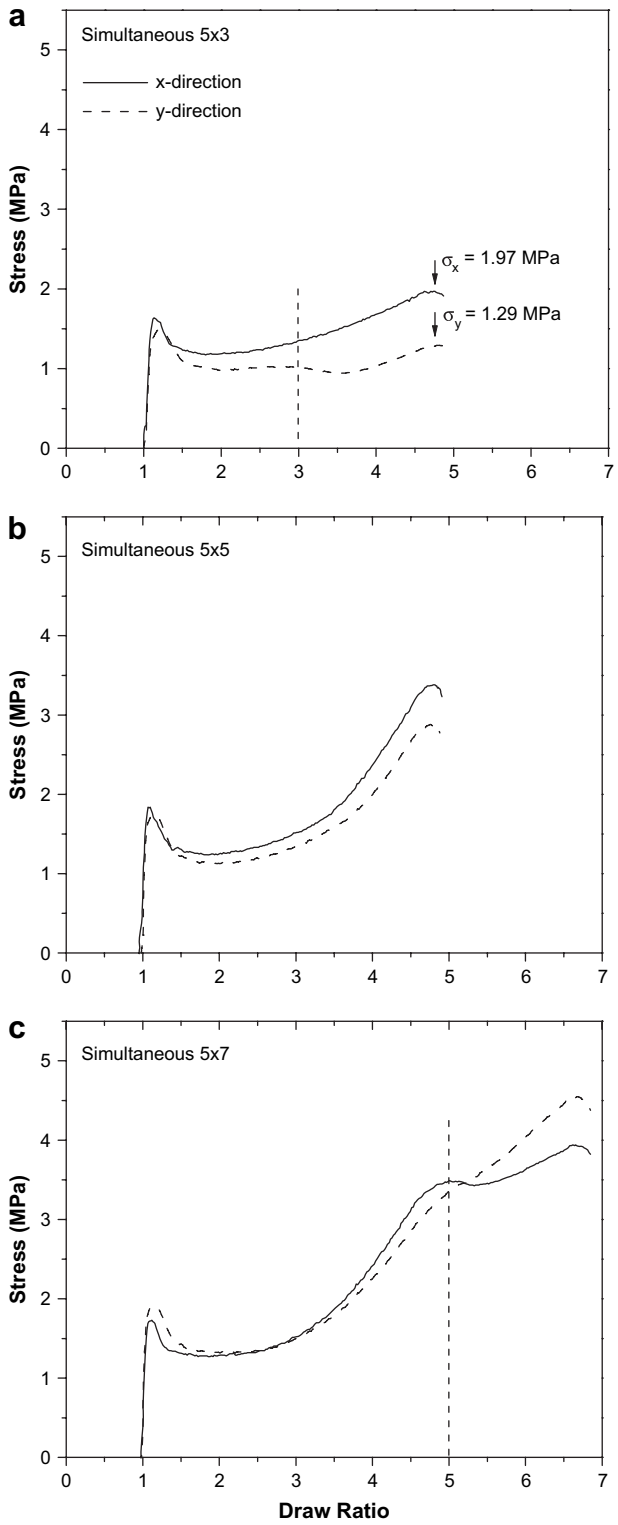

Fig. 1. Biaxial stress–strain curves for stretching simultaneously in the *x*- and *y*-direction: (a) stretched to 5 × 3; (b) stretched to 5 × 5; and (c) stretched to 5 × 7. The vertical dashed lines in (a) and (c) indicate where the film was constrained at the lower draw ratio.

x- and *y*-direction was recorded and an average final stress was calculated. It was observed that for a given biaxial draw ratio, sequential stretching led to a higher final average stress than simultaneous stretching.

A grid pattern was marked on the sheet before stretching in order to determine the uniformity of the deformation and to obtain an accurate measure of the draw ratio. Typically, the center region of the stretched film was very uniform as indicated by straight, parallel grid lines. Specimens were cut from this uniform area for further characterization. The draw ratio in the two orthogonal directions was calculated from the change in separation of the parallel grid lines. The area draw ratio A/A_o was also obtained, where A_o is the initial area defined by the grid lines and A is the area defined by the same grid lines after stretching.

3.2. Characterization of biaxially stretched films

A film that was heated at 140 °C for 60 s, which was the preheat condition used for all the stretched films, and cooled to ambient temperature without stretching was used as the control for determining the effects of stretching. Stretching reduced the density from 0.9068 g cm^{-3} for the control to almost to 0.9000 g cm^{-3} for the most highly drawn films, Fig. 3. For the same area draw ratio, sequential stretching resulted in a film of slightly lower density than simultaneous stretching. In the figure, all the sequentially stretched films followed the same trend regardless of the stretching sequence, i.e. whether the film was stretched first to the larger target draw ratio or to the smaller target draw ratio. However, it was also noted in Table 1 that unbalanced sequential stretching to the larger target draw ratio first resulted in a film with a lower density than vice versa. The difference disappeared when the data were plotted as a function of the area draw ratio because stretching to the larger target draw ratio first resulted in a film of slightly higher area draw ratio.

Crystallinity was calculated from density according to

$$X_{c,\rho} = \frac{\rho_c}{\rho}\left(\frac{\rho - \rho_a}{\rho_c - \rho_a}\right) \times 100\% \quad (2)$$

where ρ, ρ_a, and ρ_c are the bulk density, amorphous phase density, and crystalline phase density, respectively. Generally accepted values of $\rho_a = 0.853$ g cm^{-3} and $\rho_c = 0.936$ g cm^{-3} were used for the calculation [15]. The crystallinity was also calculated from the DSC heat of melting according to

$$X_{c,\,DSC} = \frac{\Delta H_m}{\Delta H_m^o} \times 100\% \quad (3)$$

where ΔH_m is the heat of melting of the specimen and 209 J g^{-1} is taken as ΔH_m^o, the heat of fusion of 100% crystallized PP [15]. Qualitatively, the DSC crystallinity followed the same trend as the density crystallinity, decreasing from about 48% for the preheated control to as low as 41% for the films with the highest draw ratios, Fig. 4a. A relatively large scatter in the DSC measurements obscured the difference between simultaneous stretching and sequential stretching that was observed in the density. To understand the decrease in crystallinity, it should be recalled that the film was partially melted during the preheat period and it remained partially melted during the stretching process. Recrystallization occurred during subsequent cooling. However, relaxation and recrystallization during cooling were inhibited by orientation of the amorphous tie chains. The decrease in crystallinity depended on how far the film had been stretched into the strain-hardening region, which underscored the effect of stretched tie chains.

The crystallinity calculated from the density was consistently higher than the crystallinity from heat of melting, Table 1. A similar discrepancy between the two crystallinity determinations is typical of polypropylene and propylene copolymers [16,17]. According to one explanation that preserves the simple two-phase model of crystalline and amorphous phases, the density of atactic polypropylene should not be used as the density of the amorphous phase in isotactic polypropylene [17]. It is proposed that constraints imposed by the crystalline phase affect chain packing in the

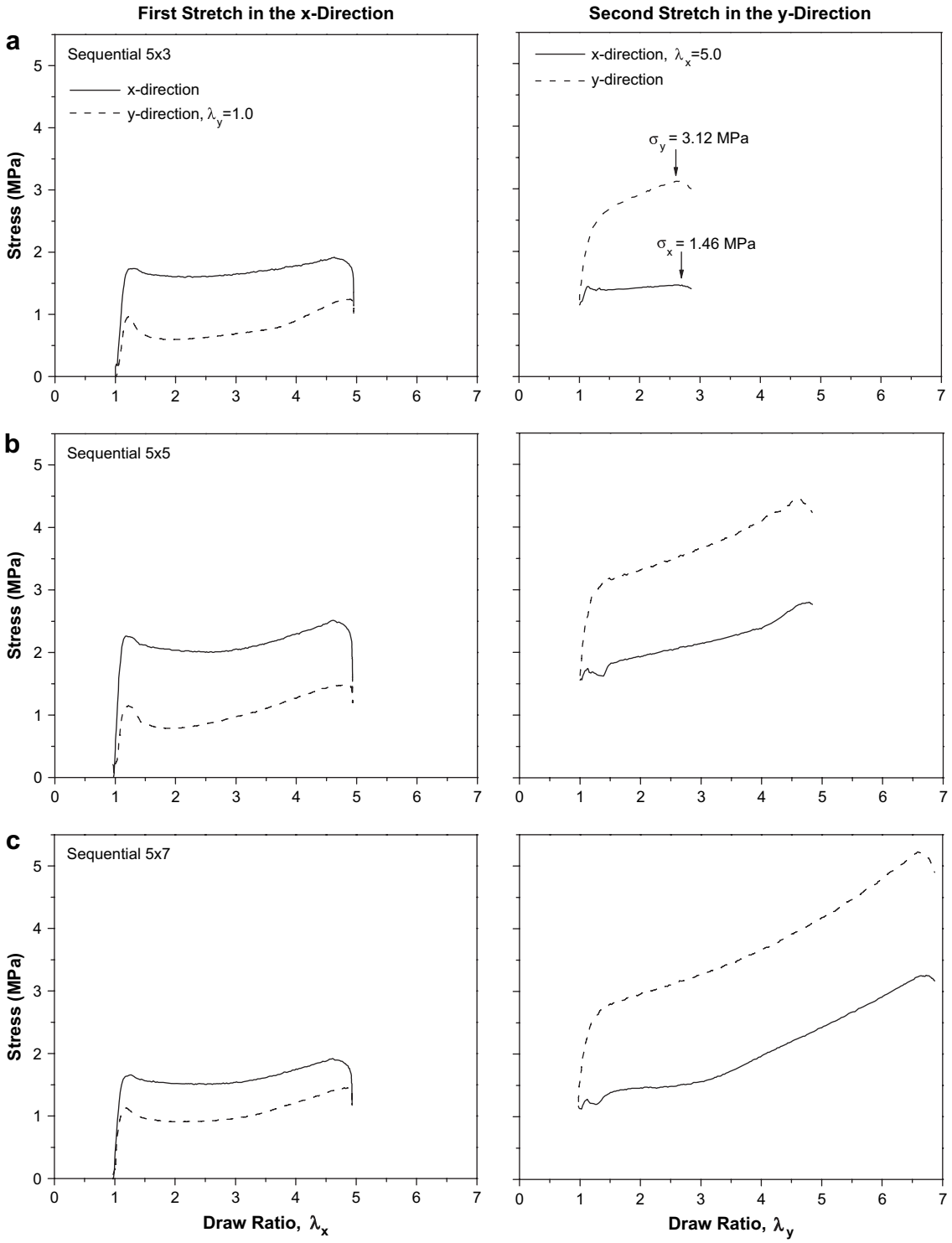

Fig. 2. Biaxial stress–strain curves for stretching sequentially in the *x*- and *y*-direction: (a) stretched to 5 × 3; (b) stretched to 5 × 5; and (c) stretched to 5 × 7.

amorphous phase and thereby increase the amorphous phase density by an amount that depends on the crystallinity. The effective amorphous phase density was calculated from the DSC crystallinity according to

$$\rho_a = \rho_c - \frac{\rho_c(\rho - \rho_c)}{\rho \times X_{c,\,DSC} - \rho_c} \tag{4}$$

As the area draw ratio increased, a decrease in density of the amorphous phase, Fig. 4b, paralleled the decrease in crystallinity, Fig. 4a. The trend was the same for simultaneously and sequentially stretched films.

Another measure of crystallinity is the total refractive index, given as

$$n_{total} = n_x + n_y + n_z \tag{5}$$

where n_x and n_y are the refractive indices in the two stretching directions and n_z is the refractive index in the normal direction. Fig. 5 shows excellent correlation between DSC crystallinity and

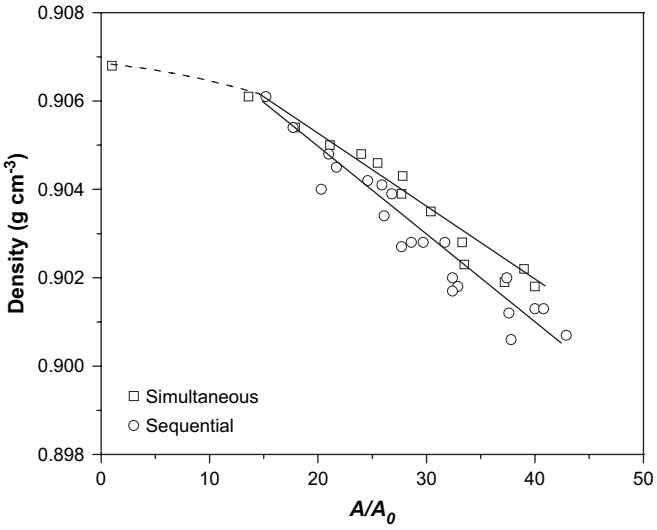

Fig. 3. Relationship between area draw ratio and density of biaxially stretched films.

crystallinity from n_{total} especially considering that the variation in crystallinity of the BOPP films is quite small.

Orientation of polymer chains is conveniently described by the birefringence index [11], which can be expressed as the normal birefringence

$$\Delta n = \frac{n_x + n_y}{2} - n_z \tag{6}$$

or as the total birefringence

$$(\Delta n_{total})^2 = \frac{1}{2}(n_x - n_z)^2 + \frac{1}{2}(n_y - n_z)^2 + \frac{1}{2}(n_x - n_y)^2 \tag{7}$$

The normal birefringence reflects the orientation with the z-direction as the reference, whereas the total birefringence measures the differences among the orientations in the x-, y- and z-direction.

To illustrate how the refractive index changed with the draw ratio, simultaneously and sequentially stretched films with $\lambda_x = 5$ were taken as example, Fig. 6. The refractive index of the unstretched control was $n_x = n_y = n_z = 1.4956$. As λ_y increased, it can be seen that n_y increased and n_x decreased. Not surprisingly, the polymer chains tended to align in the direction with the highest stretch. Concurrently, n_z also decreased although n_z decreased less than n_x. Comparing simultaneous and sequential stretching, the sequentially stretched film always had higher orientation in the y-direction and lower orientation in the x-direction for the same draw ratios, i.e. sequential stretching always gave higher orientation in the second stretch direction, and lower orientation in the first stretch direction, when compared with simultaneous stretching. For example, balanced orientation was achieved by sequentially stretching the film in Fig. 6 to 5×3.

The stretching sequence also affected the final orientation of the samples. For example, although the sequential 5×3 and 3×5 films

Table 1
Properties of BOPP films and control

	Real draw ratio	A/A_o	Density (g/cm^3)	ΔH (J/g)	$X_{c,\rho}$ (%)	$X_{c,DSC}$ (%)	n_x	n_y	n_z	$\Delta n \times 1000$	$\Delta n_{total} \times 1000$	$I_{\beta,x}$	$I_{\beta,y}$	$P(O_2)$ (Barrer)
Control	1.0 × 1.0	1.0	0.9068	101.1	66.9	48.4	1.4956	1.4956	1.4956	0.0	0.0			0.91 ± 0.02
Sim-3 × 3	3.6 × 3.7	13.6	0.9061	98.2	66.1	47.0	1.4976	1.4978	1.4885	9.1	9.1			0.88 ± 0.02
Sim-3 × 4	3.7 × 4.9	17.9	0.9054	95.8	65.3	45.9	1.4951	1.5012	1.4871	11.1	12.3	0.0349	0.0320	0.78 ± 0.00
Sim-3 × 5	3.6 × 5.9	21.1	0.9050	95.5	64.8	45.7	1.4933	1.5032	1.4867	11.6	14.4	0.0314	0.0291	0.73 ± 0.02
Sim-3 × 6	3.6 × 6.6	24.0	0.9048	95.9	64.5	45.9	1.4920	1.5041	1.4860	12.0	16.0			0.70 ± 0.00
Sim-3 × 7	3.5 × 7.8	27.8	0.9043	96.0	63.9	45.9	1.4903	1.5052	1.4854	12.4	17.9	0.0269	0.0251	0.67 ± 0.01
Sim-4 × 4	5.0 × 5.1	25.5	0.9046	96.9	64.4	46.4	1.4973	1.4985	1.4863	11.5	11.6			0.75 ± 0.00
Sim-4 × 5	4.5 × 6.2	27.7	0.9039	95.0	63.5	45.4	1.4954	1.5001	1.4861	11.6	12.3			0.75 ± 0.02
Sim-4 × 6	4.6 × 6.6	30.4	0.9035	91.8	63.0	43.9	1.4936	1.5013	1.4857	11.8	13.6			0.68 ± 0.01
Sim-4 × 7	4.5 × 7.4	33.3	0.9028	92.1	62.2	44.1	1.4921	1.5028	1.4848	12.7	15.7			0.62 ± 0.00
Sim-5 × 5	5.7 × 5.9	33.5	0.9023	92.4	61.6	44.2	1.4967	1.4975	1.4850	12.1	12.1	0.0284	0.0284	0.67 ± 0.02
Sim-5 × 6	5.6 × 6.7	37.2	0.9019	87.1	61.1	41.7	1.4952	1.4987	1.4847	12.2	12.6			0.65 ± 0.00
Sim-5 × 7	5.4 × 7.2	39.0	0.9022	90.0	61.5	43.1	1.4934	1.4999	1.4842	12.4	13.6	0.0267	0.0211	0.62 ± 0.01
Sim-6 × 6	6.3 × 6.4	40.0	0.9018	93.8	61.1	44.9	1.4966	1.4975	1.4841	12.9	12.9			0.62 ± 0.00
Seq-3 × 3	3.7 × 4.1	15.2	0.9061	98.8	66.1	47.3	1.4958	1.5006	1.4878	10.4	11.2			0.82 ± 0.05
Seq-3 × 4	3.7 × 4.8	17.7	0.9054	96.7	65.3	46.3	1.4937	1.5026	1.4866	11.6	13.9			0.75 ± 0.03
Seq-3 × 5	3.6 × 6.0	21.7	0.9045	94.8	64.3	45.4	1.4918	1.5043	1.4861	12.0	16.2	0.0329	0.0287	0.72 ± 0.05
Seq-3 × 6	3.6 × 6.8	24.6	0.9042	92.9	63.8	44.4	1.4907	1.5052	1.4853	12.7	17.8			0.67 ± 0.02
Seq-3 × 7	3.6 × 7.4	26.8	0.9039	93.0	63.5	44.5	1.4891	1.5058	1.4846	12.9	19.3			0.62 ± 0.01
Seq-4 × 3	5.0 × 4.2	21.0	0.9048	100.6	64.5	48.1	1.4973	1.4981	1.4858	12.0	12.0			0.73 ± 0.01
Seq-4 × 4	4.8 × 5.4	25.9	0.9041	99.3	63.7	47.5	1.4945	1.5005	1.4855	12.0	13.0			0.68 ± 0.00
Seq-4 × 5	4.7 × 5.6	26.1	0.9034	98.0	62.9	46.9	1.4935	1.5014	1.4856	11.9	13.7			0.70 ± 0.03
Seq-4 × 6	4.7 × 6.7	31.7	0.9028	91.2	62.2	43.7	1.4917	1.5029	1.4853	12.0	15.5			0.64 ± 0.01
Seq-4 × 7	4.5 × 7.2	32.4	0.9020	94.1	61.2	45.0	1.4903	1.5041	1.4845	12.8	17.5			0.61 ± 0.03
Seq-5 × 3	5.6 × 3.6	20.3	0.9040	95.7	63.6	45.8	1.4984	1.4964	1.4855	11.9	12.0	0.0327	0.0294	0.70 ± 0.05
Seq-5 × 4	5.5 × 5.2	28.6	0.9028	95.4	62.2	45.6	1.4955	1.4983	1.4846	12.3	12.5			0.67 ± 0.02
Seq-5 × 5	5.6 × 5.8	32.9	0.9018	85.7	61.0	41.0	1.4932	1.4987	1.4834	12.5	13.4	0.0264	0.0259	0.61 ± 0.00
Seq-5 × 6	5.6 × 6.7	37.6	0.9012	89.0	60.4	42.6	1.4921	1.5008	1.4835	13.0	15.0			0.59 ± 0.00
Seq-5 × 7	5.5 × 7.3	40.0	0.9013	90.1	60.4	43.1	1.4903	1.5015	1.4830	12.9	16.1	0.0188	0.0177	0.58 ± 0.00
Seq-6 × 3	6.6 × 4.2	27.7	0.9027	94.5	62.1	45.2	1.5007	1.4961	1.4850	13.4	13.9			0.67 ± 0.01
Seq-6 × 4	6.5 × 5.0	32.4	0.9017	94.0	60.9	45.0	1.4968	1.4971	1.4846	12.4	12.4			0.62 ± 0.01
Seq-6 × 5	6.4 × 5.9	37.8	0.9006	89.9	59.6	43.0	1.4949	1.4988	1.4836	13.3	13.7			0.59 ± 0.00
Seq-6 × 6	6.3 × 6.8	42.9	0.9007	90.2	59.7	43.1	1.4931	1.4998	1.4832	13.3	14.5			0.56 ± 0.02
Seq-7 × 3	7.3 × 4.1	29.7	0.9028	91.2	62.2	43.7	1.5005	1.4936	1.4850	12.0	13.5			0.64 ± 0.00
Seq-7 × 4	7.2 × 5.2	37.4	0.9020	91.7	61.2	43.9	1.4974	1.4956	1.4842	12.3	12.4			0.58 ± 0.01
Seq-7 × 5	7.1 × 5.8	40.8	0.9013	90.9	60.4	43.5	1.4959	1.4965	1.4835	12.7	12.7			0.55 ± 0.00

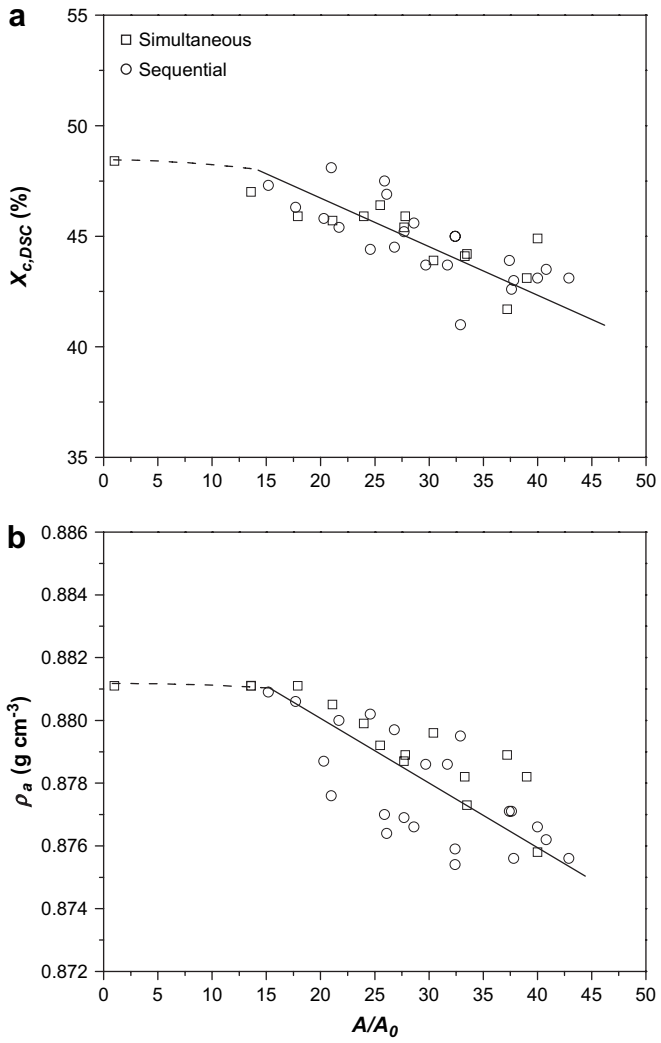

Fig. 4. Effect of area draw ratio on: (a) crystallinity from DSC and (b) amorphous phase density.

have similar area draw ratios (21.7 and 20.3), the 5×3 film showed almost balanced orientation whereas the 3×5 film had much higher orientation in the second stretch direction, Table 1. It can be imagined that constrained *y*-direction yielding during *x*-direction stretching facilitated the processes of chain orientation when the film was subsequently stretched in the *y*-direction. This also could have been the origin of the anisotropic fiber morphology reported by others [4].

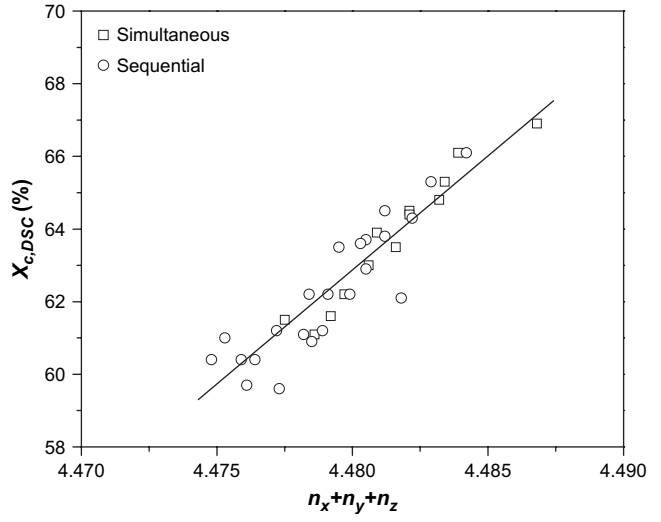

Fig. 5. Relationship between the total refractive index and the crystallinity from DSC.

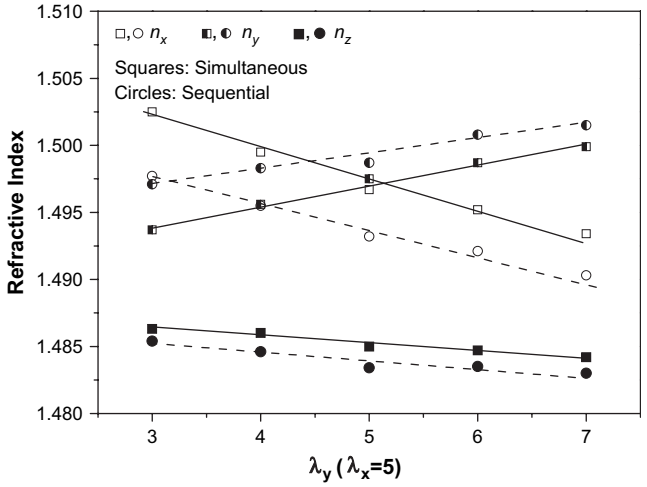

Fig. 6. Effect of λ_y for constant $\lambda_x = 5$ on refractive indices of simultaneously and sequentially biaxially stretched films.

3.3. Oxygen permeability of biaxially stretched films

Increasing the draw ratio of the stretched film had the effect of reducing the oxygen permeability, Fig. 7. The effect was slightly higher with sequential stretching, which was consistent with the general finding that the sequential stretching produced a somewhat larger effect than simultaneous stretching at the same draw ratio.

According to free volume concepts of gas transport as applied to the two-phase model for crystalline polymers, the crystals are considered impermeable and diffusion occurs through the amorphous phase free volume. These concepts readily account for the general observations that gas permeability is reduced by increasing the crystallinity and by increasing the amorphous phase density [18]. However, for the stretched films, the decrease in permeability was accompanied by decreasing density, which combined lower crystallinity (more amorphous phase) and lower

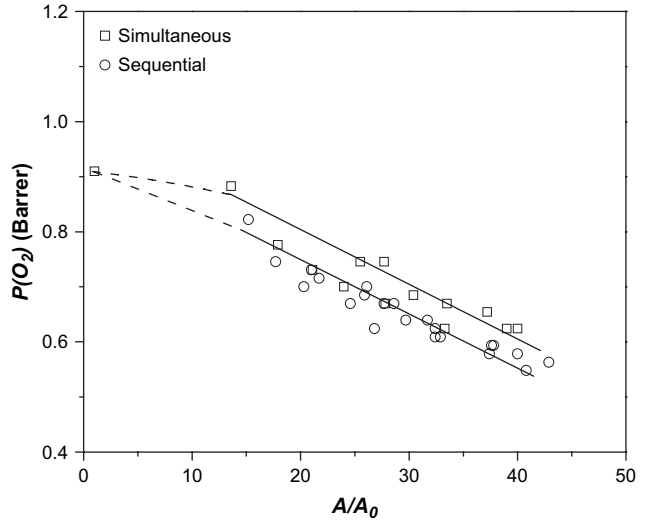

Fig. 7. Relationship between area draw ratio and oxygen permeability of biaxially stretched films.

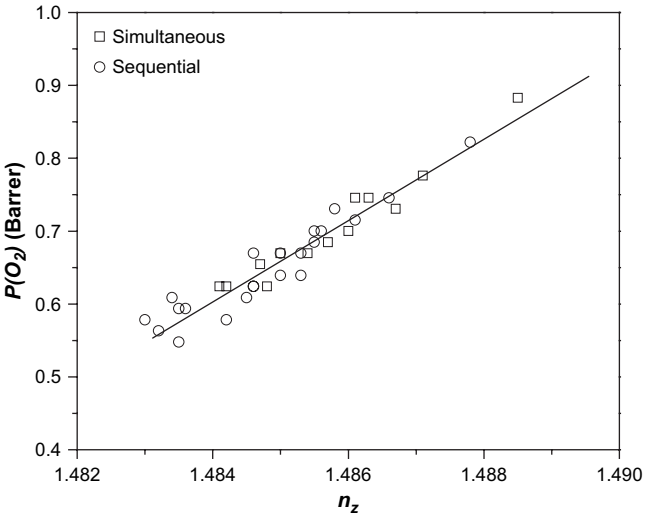

Fig. 8. Relationship between oxygen permeability and refractive index in the *z*-direction.

amorphous phase density (higher free volume) (see Fig. 4a,b). This result appeared to be inconsistent with conventional free volume concepts of gas permeability. It was possible that stretching in the pre-melting region indeed decreased the size of nanoscale free volume holes, but at the same time introduced a population of submicron voids. The former would have decreased the gas permeability, whereas the latter would have decreased the density without affecting the gas diffusivity. Although this possibility could not be ruled out completely, previous positron annihilation lifetime spectroscopy measurements on similar films showed that the stretching conditions did not affect the free volume hole size [13]. Thus, some other factor or factors overrode the effects of density alone.

The two-phase transport model is appropriate for isotropic films, but does not consider the effects of orientation. No general trend is found in the relationship between permeability and Δn_{total}, Table 1. For these films, Δn_{total} is determined primarily by the difference between n_x and n_y. The normal birefringence reflects the orientation with the *z*-direction as the reference. In general, *P* of the stretched films decreases with increasing orientation as measured by Δn, Table 1. A better correlation is observed between *P* and n_z, Fig. 8. However, it was demonstrated that the correlation between *P* and n_z depends on the resin [13], and the thermal history of the compression molded sheet [14]. This is understandable because *n* includes a large contribution from the crystalline phase orientation. A parameter that reflects the properties of the amorphous phase only is needed.

It was previously found that the decrease in oxygen permeability of stretched films was due primarily to a decrease in the diffusivity [19]. According to the free volume concepts of gas transport, diffusivity derives from the dynamic free volume. A reduction in amorphous chain mobility can lead to lower diffusivity by decreasing the frequency with which connecting channels form between free volume holes. In particular, chain mobility in the *x*- and *y*-direction provides the channels perpendicular to the *z*-direction that allow gas molecules to diffuse. In polypropylene, main chain mobility in the amorphous phase is associated with the dynamic mechanical β-relaxation at about 10 °C. To obtain the intensity of the β-relaxation, the tan δ curve is deconvoluted into 3 Gaussian contributions from the β-relaxation, the α-relaxation and the onset of melting as illustrated with a film that was simultaneously stretched to 5 × 7 in Fig. 9. The intensity of the β-relaxation I_β is taken as the height of the deconvoluted peak.

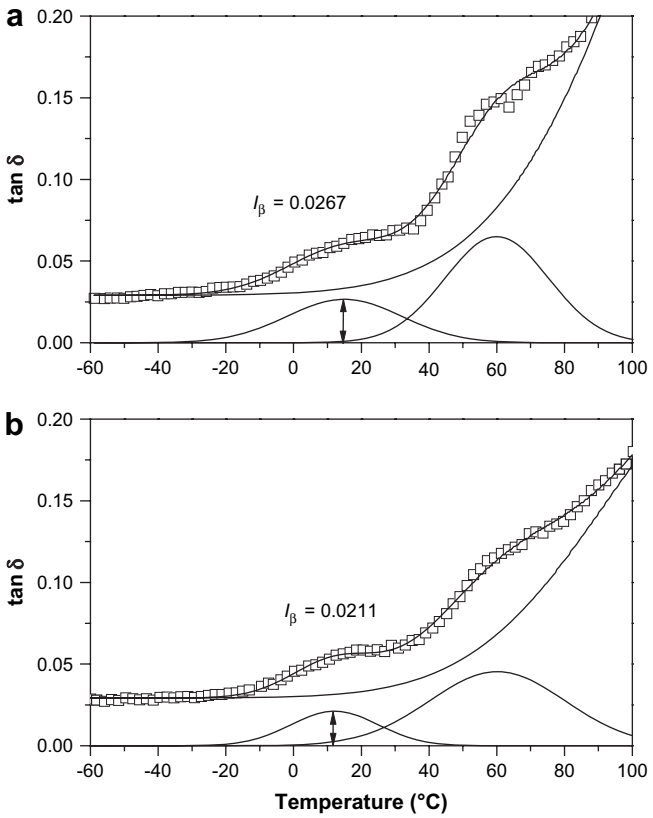

Fig. 9. DMTA spectra of a film simultaneously stretched to 5 × 7: (a) the *x*-direction and (b) the *y*-direction.

Because the permeability measurement combined the effects of orientation in both *x*- and *y*-direction, the average value of I_β was used to characterize the chain mobility. The permeability of some simultaneously and sequentially stretched films is plotted against the average I_β in Fig. 10. Previous results on stretched films prepared from compression molded sheets of the same resin with different thermal histories [14], and results from stretched films of different resins, including a metallocene PP and a propylene/ethylene copolymer [13], are included. All the data fit a good linear relationship between permeability and chain mobility as reflected by I_β from DMTA. The extrapolated oxygen permeability at zero I_β

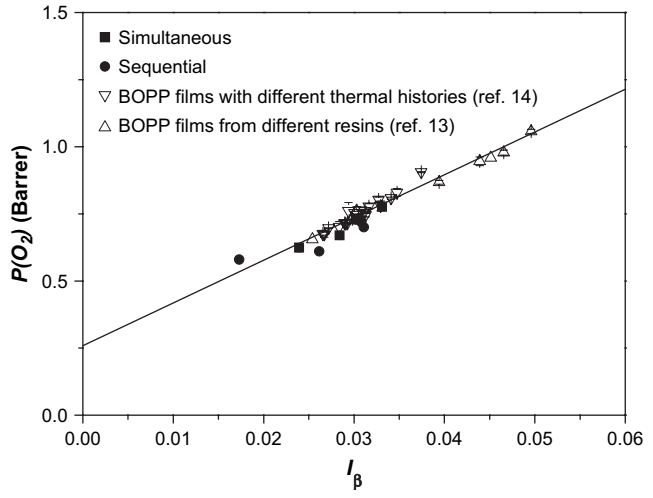

Fig. 10. Relationship between oxygen permeability and the β-relaxation intensity averaged in the *x*- and *y*-direction.

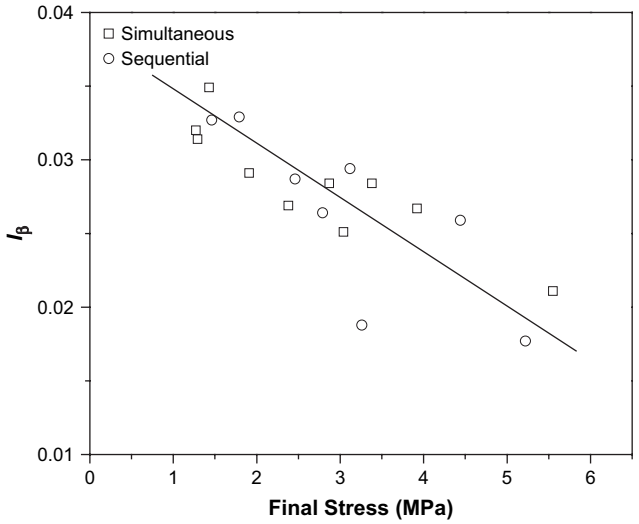

Fig. 11. Relationship between the β-relaxation intensity and the final stress when the film achieved the target draw ratio with results for the *x*- and *y*-direction plotted separately.

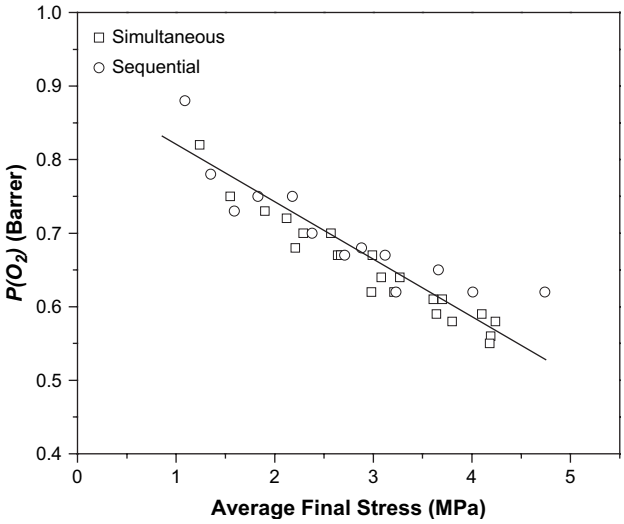

Fig. 12. Relationship between the oxygen permeability and the final stress averaged in the *x*- and *y*-direction.

(0.26 Barrer) was the contribution from relaxations that were active below the temperature of the β-relaxation [14].

For the film illustrated in Fig. 9 that was simultaneously stretched to 5×7, I_β was lower in the direction of higher draw ratio. Not surprisingly, this was the case for all the films that were simultaneously stretched to an unbalanced draw ratio. However, the sequentially stretched films did not necessarily follow this trend. Rather, the I_β was lower in the second stretch direction regardless of whether λ_y was larger or smaller than λ_x, Table 1. Thus, the second stretch was more effective than the first in orienting the amorphous chains. Refractive index, which reflected primarily the crystalline orientation, revealed that sequential stretching always gave higher orientation in the second stretch direction, and lower orientation in the first stretch direction, when compared with simultaneous stretching. The I_β results revealed that the second stretching was also more effective than the first in stretching and tightening the amorphous chains. It may be that constrained yielding during the first stretching facilitated subsequent orientation during the second stretching.

In biaxial stretching, orientation occurred during strain hardening by the processes of lamellar breakup and recrystallization. Although recrystallization of impermeable crystals as high aspect ratio, oriented platelets could have contributed to the decrease in permeability, orientation also stretched and tightened the amorphous tie chains that connected the crystals and transferred the stress. Parallel changes in P and n_z (see Fig. 8) were attributed to increasingly taut tie molecules as the process of crystalline orientation proceeded. The amount of crystalline phase orientation, and the extent to which the tie chains were stretched and tightened, depended on the stress applied to the film. This suggested a relationship between the β-relaxation intensity and the stress when the film achieved the final draw ratio. Fig. 11 shows the relationship between I_β and the final stress with the *x*- and *y*-direction results plotted separately. Clearly, a higher stress during stretching resulted in a lower I_β, which translated to lower gas permeability.

It was now possible to establish a relationship between the oxygen permeability of the biaxially stretched film and the stress on the film during stretching. Because the permeability measurement combined the effects of stretching in both *x*- and *y*-direction, the average final stress was used to test the relationship. The result in Fig. 12 confirmed a systematic decrease in P as the film experienced increasingly higher stresses during stretching. As with relationships between P and n_z, the final stress was expected to depend on the resin and the thermal history of the compression molded sheet used to prepare the stretched film. However, it should be useful for predicting the relative gas permeability from the knowledge of the stress applied during stretching without the need to measure I_β.

4. Conclusions

Characterization of the BOPP films revealed significant differences between simultaneous and sequential stretching. Sequential drawing always gave higher orientation in the second stretch direction, and lower orientation in the first stretch direction, when compared with simultaneous stretching to the same biaxial draw ratios. It followed that in sequential stretching to unbalanced draw ratios, different results were obtained depending upon whether the first stretch was taken to the larger or the smaller draw ratio. It was imagined that constrained yielding in the second stretch direction during stretching in the first direction facilitated the processes of chain orientation when the film was subsequently stretched in the second direction.

This study also tested the generality of a one-to-one correlation between the oxygen permeability of BOPP films and the intensity of the dynamic mechanical β-relaxation. The study demonstrated that the correlation extends to commercially important sequentially drawn BOPP films with an unbalanced draw ratio. Unlike the total orientation as measured by birefringence, the intensity of the β-relaxation is specific to the amorphous phase and therefore a single correlation applies to different resins and to different thermal histories. Despite increases in the amount of amorphous phase (decreased crystallinity) and in the amount of free volume (decreased amorphous phase density), the oxygen permeability decreased with increasing area draw ratio. The result appeared to be inconsistent with conventional free volume concepts of gas permeability. Rather, the controlling factor was thought to be the reduced mobility of stretched tie chains that control the frequency with which connecting channels form between free volume holes. The extent to which the tie chains were stretched and tightened depended on the stress applied to the film. This resulted in a systematic decrease in P as the film experienced increasingly higher stresses during stretching. Although the stress on the stretched

film was expected to depend on the resin and the thermal history of the sheet used to prepare the stretched film, nevertheless, the relationship should be useful for predicting the relative gas permeability from the knowledge of the stress applied during stretching.

Acknowledgements

The authors thank The Dow Chemical Company for generous technical and financial support.

References

[1] Phillips RA, Nguyen T. J Appl Polym Sci 2001;80:2400–15.
[2] Dias P, Hiltner A, Baer E, Van Dun J, Chen HY, Chum SP. Annual technical conference, vol. 64. Society of Plastics Engineers; 2006. p. 2660–4.
[3] Breil J. Annual technical conference, vol. 60. Society of Plastics Engineers; 2002. p. 2501–5.
[4] Lüpke T, Dunger S, Sanze J, Radusch HJ. Polymer 2004;45:6861–72.
[5] Okajima S, Kurihara K, Keisuke H. J Appl Polym Sci 1967;11:1703–17.
[6] Nie HY, Walzak MJ, McIntyre NS. Polymer 2000;41:2213–8.
[7] Karacan I, Taraiya AK, Bower DI, Ward IM. Polymer 1993;34:2691–701.
[8] Masuko T, Tanaka H, Okajima S. J Polym Sci Part A-2 1970;8:1565–74.
[9] Tanaka H, Masuko T, Okajima S. J Polym Sci Part A-1 1969;7:3351–61.
[10] Rizzo P, Venditto V, Guerra G. Macromol Symp 2002;185:53–63.
[11] Taraiya AK, Orchard GAJ, Ward IM. J Appl Polym Sci 1990;41:1659–71.
[12] Taraiya AK, Orchard GAJ, Ward IM. J Polym Sci Part B Polym Phys 1993;31:641–5.
[13] Dias P, Lin YJ, Hiltner A, Baer E, Chen HY, Chum SP. J Appl Polym Sci 2008;107:1730–6.
[14] Lin YJ, Dias P, Chen HY, Chum S, Hiltner A, Baer E. Polym Eng Sci 2008;48:642–8.
[15] Brandrup J, Immergut EH. Polymer handbook. 3rd ed. New York: Wiley; 1989 [Section V/27].
[16] Isasi JR, Mandelkern L, Galante MJ, Alamo RG. J Polym Sci Part B Polym Phys 1999;37:323–34.
[17] Wang HP, Ansems P, Chum SP, Hiltner A, Baer E. Macromolecules 2006;39:1488–95.
[18] Hiltner A, Liu RYF, Hu YS, Baer E. J Polym Sci Part B Polym Phys 2005;43:1047–63.
[19] Somlai LS, Liu RYF, Landoll LM, Hiltner A, Baer E. J Polym Sci Part B Polym Phys 2005;43:1230–43.